DELAYED RECTIFICATION IN THE CALF CARDIAC PURKINJE FIBER

Evidence for Multiple State Kinetics

PAUL B. BENNETT, LESLIE C. MCKINNEY, ROBERT S. KASS, AND TED BEGENISICH
University of Rochester, School of Medicine and Dentistry, Department of Physiology, Rochester, New York 14642

ABSTRACT We have investigated the delayed rectifier current (I_x) in the calf cardiac Purkinje fiber using a conventional two-microelectrode voltage clamp arrangement. The deactivation of I_x was monitored by studying decaying current tails after the application of depolarizing voltage prepulses. The reversal potential (V_{rev}) of these I_x tails was measured as a function of prepulse magnitude and duration to test for possible permeant ion accumulation- or depletion-induced changes in V_{rev}. We found that prepulse-induced changes in V_{rev} were <5 mV, provided that prepulse durations were ≤3.5 s and magnitudes were ≤+35 mV. We kept voltage pulse structures within these limits for the remainder of the experiments in this study. We studied the sensitivity of V_{rev} to variation in extracellular K^+. The reversal potential for I_x is well described by a Goldman-Hodgkin-Katz relation for a channel permeable to Na^+ and K^+ with P_{Na}/P_K = 0.02. The deactivation of I_x was always found to be biexponential and the two components shared a common reversal potential. These results suggest that it is not necessary to postulate the existence of two populations of channels to account for the time course of the I_x tails. Rather, our results can quantitatively be reproduced by a model in which the I_x channel can exist in three (two closed, one open) conformational states connected by voltage dependent rate constants.

INTRODUCTION

Repolarization of action potentials in cardiac cells depends upon time-dependent changes in small inward and outward currents and can be dramatically modified by slight changes in individual current components (Noble and Tsien, 1972). In nerve and skeletal muscle, delayed rectifier potassium channels responsible for action potential repolarization have been well characterized (reviewed by Latorre and Miller, 1983). The properties of the repolarizing outward current in cardiac preparations, also referred to as delayed rectification, are not as well understood.

Noble and Tsien (1969) analyzed a time-dependent outward current present during the plateau phase of the action potential in sheep cardiac Purkinje fibers. Based on limited data, they suggested that this current was carried at least partially by potassium ions, but because other ions were thought to contribute to the current, it was labeled I_x. Two components of I_x (I_{x1} and I_{x2}) were observed and distinguished by their kinetics and selectivity. Other similar outward currents have since been reported in several types of cardiac cells (Brown and Noble, 1969; Ojeda and Rougier, 1974; McGuigan, 1974; McDonald and Trautwein, 1978; Noma and Irisawa, 1976; Meier and Katzung, 1981; Isenberg and Klockner, 1982*a*; Hume, 1983; Green et al., 1983).

Investigation of membrane current in cardiac preparations has been hampered by several problems, such as overlapping time- and voltage-dependent currents, spatial voltage-nonuniformity, and the possibility of ion accumulation and/or depletion in restricted extracellular spaces. In fact, it has been suggested that the current called I_{x2}, which has been investigated using very long-lasting depolarizations, might be an artifact due to ion accumulation or depletion in a restricted extracellular space (Noble and Tsien, 1969; McGuigan, 1974; Noble, 1976; McDonald and Trautwein, 1978). In addition to these difficulties, disruption of indigenous mechanisms that regulate cellular calcium causes the intracellular calcium concentration to oscillate and produce fluctuations in membrane current (Colquhoun et al., 1981; Kass and Tsien, 1982; Wier et al., 1983; Allen et al., 1984). The presence of these Ca-dependent oscillations masks small membrane currents such as I_x and precludes their analysis (Jaeger and Gibbons, 1981).

The introduction of the enzymatically dispersed, single cardiac cell as a viable electrophysiological preparation has helped solve many of these problems. However, these cells also present experimental limitations. In long-lasting experiments, single cells are especially vulnerable to Ca overload, and thus to Ca-dependent current fluctuations (Dani et al., 1979; Isenberg and Klockner, 1982*b*; Murphy

et al., 1983). Furthermore, it is very important to determine whether enzymatic digestion, used to isolate cardiac cells, causes significant changes in the properties of membrane currents or modifies their response to hormones, such as epinephrine.

The purpose of this study was to investigate the delayed rectifier in the calf cardiac Purkinje fiber under experimental conditions that address the above problems. We chose the calf Purkinje fiber because it is one of the few cardiac preparations in which each of these experimental difficulties has been, or can be, addressed. Previous work has shown that voltage control is adequate for the measurement of membrane conductance 10 times larger than the I_x conductance (Kass et al., 1979); pharmacological probes have been identified that block the two overlapping plateau currents, calcium channel current (I_{Ca}), and transient outward current (I_{to}), but not I_x (Kass, 1982, 1984); and membrane current fluctuations, driven by internal calcium levels, have been quantitatively investigated and can thus be avoided (Kass and Tsien, 1982) in the calf Purkinje fiber.

We have tested for and found experimental conditions under which accumulation or depletion of charge carrier does not complicate the analysis of the delayed rectifier, I_x. Our experiments were designed to quantitatively characterize the ion selectivity, voltage dependence, and kinetic properties of the delayed rectifier. The results of this study can be compared with the properties of delayed rectification observed in other cardiac preparations, such as enzymatically dispersed cells and rabbit or canine Purkinje strands. A preliminary report of these findings was presented to the Biophysical Society (Bennett et al., 1984).

METHODS

Preparation and Recording

Calf hearts, obtained at a local slaughterhouse, were transported to the laboratory in ice-cold, oxygenated Tyrode's solutions (see Scheuer and Kass, 1983 for details). Purkinje fiber cell bundles were isolated from both ventricles. Membrane current was recorded from shortened cell bundles (1–1.5 mm long, 100–200 μM diameter). Microelectrodes were pulled from omega-dot glass (1.2 mm o.d. × 0.9 mm i.d., Glass Co. of America, Bargaintown, NJ) and bevelled with a modified spin bar beveller (Kass and Bennett, 1985). The electrodes were arranged to optimize measurement of outward current (Kass et al., 1979). Voltage recording electrodes were filled with 3 M KCl, and current passing electrodes were filled with 1.5 M K citrate.

Voltage-clamp Techniques

The voltage clamp of these shortened Purkinje fibers was accomplished with the two-microelectrode arrangement. This technique has been compared with the three-microelectrode method, and its adequacy examined both experimentally and theoretically (Kass et al., 1979). This analysis showed that the two-electrode technique provides accurate measurement of Ca channel current in these fibers. Since Ca channel currents are much larger and faster than the delayed rectifier currents, these currents are likewise expected to be accurately measured.

However, since we used elevated potassium concentrations in this paper, we analyzed the quality of voltage control under conditions appropriate for our experiments with a model previously described in detail by Kass et al. (1979) and Kass and Bennett (1985).

Briefly, a short segment of a Purkinje fiber is simulated as a one-dimensional cable consisting of 21 interconnected segments containing voltage- and time-dependent conductances. For the present work both calcium and I_x conductances are represented as well as a time- and voltage-independent leakage conductance. For computational purposes, the calcium conductance is approximated as a two-time constant (activation/inactivation) process and I_x as a single time constant element.

The results of the computation are summarized in Fig. 1. The figure shows one half of a simulated 2-mm short cable model of the Purkinje fiber. Voltage distributions are symmetrical about the current passing electrode located at $X = 0$ in the computation. Computed voltages are illustrated as functions of time at three different positions along the cable: 0.15, 0.30, and 0.65 mm from the current electrode. A command pulse from 0 to +50 mV (relative to the resting potential) is imposed at the location 0.65 mm from the current electrode. Panel *A* shows these voltages for our simulated normal K_o conditions, in which we have assumed an I_x conductance ~10 times greater than we measure experimentally. Thus, this represents a worst-case situation. Voltages rises rapidly along the cable and the small (1 mV) voltage gradient that exists in the steady state does not distort the two-electrode measurement of membrane current.

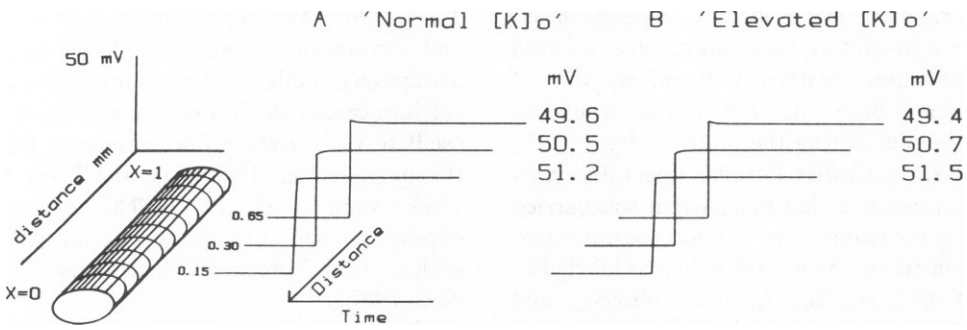

FIGURE 1 Computational test of the effects of elevated K_o concentrations on voltage control. I_x was assumed to be zero at rest, fully activated in the steady state at the test voltage, and was given a 100-ms activation time constant. The voltage steps shown were 800 ms in duration. Time constants for activation and inactivation of I_{Ca} were assumed to be 5 and 20 ms, respectively, and the fully activated Ca conductance was 0.8 mmhos/cm^2. The I_{Ca} reversal potential was set at +140 mV. Voltages are shown as functions of time at three locations (0.15, 0.30, and 0.65 mm from the current electrode) along the cable. (*A*) Normal K_o conditions. The I_x reversal potential was 0 mV (resting potential) and the maximal conductance (G_x) was 0.3 mmhos/cm^2. The leak conductance was 0.1 mmhos/cm^2. (*B*) Elevated K_o conditions. The leak conductance was doubled, G_x was changed to 0.4 mmhos/cm^2, and the I_x reversal potential was shifted by +40 mV.

Fig. 1 *B* shows the same type of computation with the I_x and leak conductance increased, and the I_x reversal potential made 40 mV more positive. These conditions simulate elevated external potassium concentration. Even under these conditions the voltage changes rapidly and uniformly over the length of the fiber and the two-electrode technique accurately measures membrane current.

Data Acquisition

Membrane currents in most of the experiments in this study were sampled by a 12 bit analog/digital converter controlled by a microcomputer of our own design. Typically, sampling frequency (time) of 143 Hz (7 ms) was used with the currents filtered by a low-pass, eight-pole Bessel filter of 40 Hz, equivalent to a time constant of 4 ms, which will have a negligible effect on even the fastest measured time constants of 50 ms. Indeed, filtering at higher frequency only increased background noise and did not alter the time course of I_x currents. The voltage protocols were also generated by this computer system.

In some experiments data were recorded on a Brush 2400 chart recorder (Gould Instrument Div., Cleveland, OH). In these experiments the currents were filtered at 50 Hz. Voltage clamp pulses were generated by a WPI pulse generator (World Precision Instruments, New Haven, CT).

Solutions

The standard modified Tyrode's solution contained 150 mM NaCl, 4 mM KCl, 5 mM glucose, 1.8 mM $CaCl_2$, 0.5 mM $MgCl_2$, and 10 mM Tris-HCl (pH = 7.4). Changes in external K^+ concentrations were made by adding appropriate aliquots of a concentrated KCl stock solution to K^+-free Tyrode's solutions. In experiments that required elevation of KCl above 20 mM, the concentration of NaCl was reduced to maintain osmotic balance. Temperature was regulated with a thermoelectric device (Cambion, Cambridge, MA) over a temperature range of 35–37°C, with temperature kept constant to within ±0.5°C during any given experiment.

Pulse Protocols and Data Analysis

Three protocols described by Noble and Tsien (1969) were used to assay changes in I_x. In each protocol, decaying current tails were measured at a particular potential after applying a conditioning voltage of appropriate magnitude and duration. A general function with two exponentials plus a baseline

$$y(t) = A_1 e^{-t/\tau 1} + A_2 e^{-t/\tau 2} + A_3 \qquad (1)$$

was fitted to each current tail, using an algorithm for least squares estimation of nonlinear parameters (Levenberg, 1944; Marquardt, 1963; Bevington, 1969). Values of A_1 and A_2 correspond to the amplitude of each component of I_x at time zero, the end of the conditioning voltage. Total tail current amplitude is equal to the sum of A_1 and A_2.

Current tails in reversal potential experiments were measured at a series of potentials after applying a conditioning pulse of fixed amplitude and duration. Current-voltage relationships for I_x could then be determined by plotting tail amplitude (measured as described above) against test potential.

In the second type of protocol, used to determine the time course of activation of I_x, prepulses were applied to a common test potential for various durations. Current tails were measured at the holding potential after each prepulse and the amplitude of each tail plotted against prepulse duration. The resulting envelope of tail current magnitudes was used as an assay of the time course of I_x activation that occurs at the prepulse voltage. The envelope of tails was fitted with an exponential function, using the nonlinear least squares fitting procedure described above.

In the third protocol, used to determine the voltage dependence of I_x activation, prepulse magnitude was varied at constant duration. Tail current amplitudes, measured at the holding potential, are proportional to the conductance at the end of the prepulse. The voltage-dependence of these tail current amplitudes, then, is a measure of the voltage-dependence of activation of I_x channels.

Separation of Overlapping Ionic Currents

Positive holding potentials (usually near −30 mV) were chosen to inactivate sodium channel currents (Colatsky, 1980) and to partially inactivate calcium channel currents (Reuter, 1979) and the transient outward current (Fozzard and Hiraoka, 1973; Siegelbaum and Tsien, 1980). Voltages were chosen to avoid time-dependent currents in the pacemaker range of potentials (Noble and Tsien, 1968; DiFrancesco, 1981).

The fastest time constants measured in our experiments were slower than 50 ms; much too slow to be significantly contaminated by calcium channel currents, which deactivate with time constants <3 ms in single cells (Lee and Tsien, 1983) and are too fast to resolve in multicellular preparations (Kass and Sanguinetti, 1984). Furthermore, our currents have reversal potentials in the range −70 to −20 mV (depending upon external potassium concentration), which is much more negative than the calcium channel reversal reported for single cardiac cells (Lee and Tsien, 1982) and multicellular preparations (Reuter and Scholz, 1977; Kass and Sanguinetti, 1984). We thus expected little, if any, contamination of our measurements by calcium channel currents not already inactivated by the depolarized holding potential.

However, we also carried out experiments with nisoldipine, a dihydropyridine Ca channel blocker, to confirm that our measurements are not contaminated by Ca sensitive currents (I_{to} and I_{Ca}). Nisoldipine has been shown to block both I_{to} and I_{Ca} but not I_x in calf Purkinje fibers (Kass, 1982, 1984). Recent experiments have shown this drug to be especially potent when it is applied to preparations maintained at depolarized holding potentials, such as those used in this study (Sanguinetti and Kass,

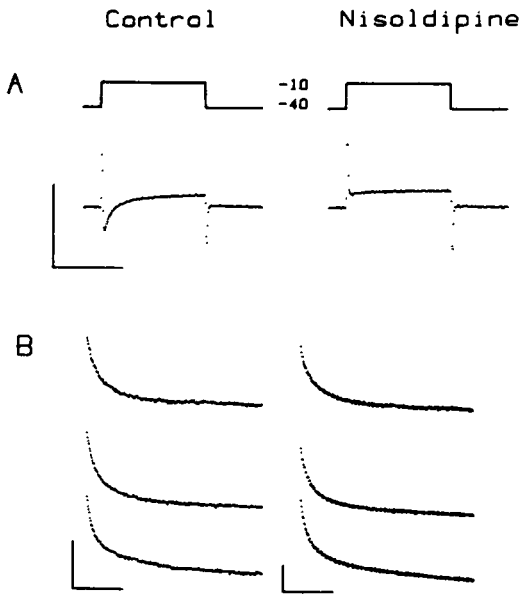

FIGURE 2 Nisoldipine: a pharmacological test for contamination of I_x tails by Ca-sensitive currents. (*A*) Ca channel currents, apparent in control conditions (*left*), are blocked by nisoldipine (100 nM) (*right*) at −40 mV holding potential. Calibration bars: 60 nA, 200 ms. (*B*) I_x tail currents measured at potentials in the absence (*left*) and presence (*right*) of nisoldipine (50 nM). Control records are from preparation AL12 and the drug records obtained, after changing perfusate to drug-containing solution, are from preparation BU4. Current tails were recorded at −20, −30, and −40 mV (top to bottom) after 0.8 s prepulses to +10 mV (control) and +13 mV (nisoldipine). Calibration bars: 5 nA, 0.5 s.

1984). Consequently, we were able to use very low concentrations of nisoldipine to block I_{to} and I_{Ca} and then measure I_x. We reasoned that if our measurements of I_x tail currents in drug-free conditions were distorted by these other plateau currents, differences would emerge between records obtained in the absence and presence of nisoldipine.

Fig. 2 illustrates the results we typically obtained in the comparison of drug-containing and drug-free current records. Panel *A* illustrates the influence of nisoldipine (100 nM) on membrane currents measured during relatively brief depolarizing voltage pulses. Nisoldipine blocks the Ca-dependent currents, I_{Ca} and I_{to}. Close examination of the current recorded after the depolarizing pulses shows small outward current tails in the absence and presence of nisoldipine (see also Kass, 1984, Fig. 2). The insensitivity of I_x tails to nisoldipine is more apparent in panel *B*, which shows a set of I_x tail records obtained in the absence and presence of nisoldipine after similar prepulses in two separate preparations.

We compared I_x tail currents measured in the presence of nisoldipine (a total of five experiments) to those in the absence of drug and found no differences in I_x kinetics. These results, summarized in Fig. 8, support the previously reported insensitivity of the I_x activation curve to nisoldipine (Kass, 1982, 1984).

In summary, we have used depolarized holding potentials (near −30 mV) in this study to reduce I_{to} and I_{Ca} and eliminate I_{Na} via inactivation. The experiments done with nisoldipine support the point that any current that might remain through the I_{Ca} and I_{to} channels must have faster kinetics than the I_x currents. Thus, we conclude that our measurements, even in the absence of nisoldipine, are not contaminated by the overlapping plateau currents.

RESULTS

Potassium Accumulation Can Be Minimized

Our initial experiments were designed to define conditions that would minimize artifacts due to extracellular ion accumulation or depletion. It was reasoned that concentration changes in a restricted extracellular space would be manifested as changes in the I_x reversal potential (for example, see Beam and Donaldson, 1983*b*).

In the experiment illustrated in Fig. 3, depolarizing conditioning pulses were applied to activate I_x. The reversal potential of I_x tail currents was measured for conditioning pulses to +10 mV for durations of 0.6, 1.5, and 3 s. The longer pulses prolonged current flow through the I_x channels and provided conditions that could have promoted ion accumulation or depletion. However, the reversal potential, V_{rev}, was not affected by these changes in prepulse duration (Fig. 3 *A*). This point is more clearly demonstrated in Fig. 3 *B* by the common reversal potential of the current-voltage relations for each prepulse duration.

This experiment was repeated with several different

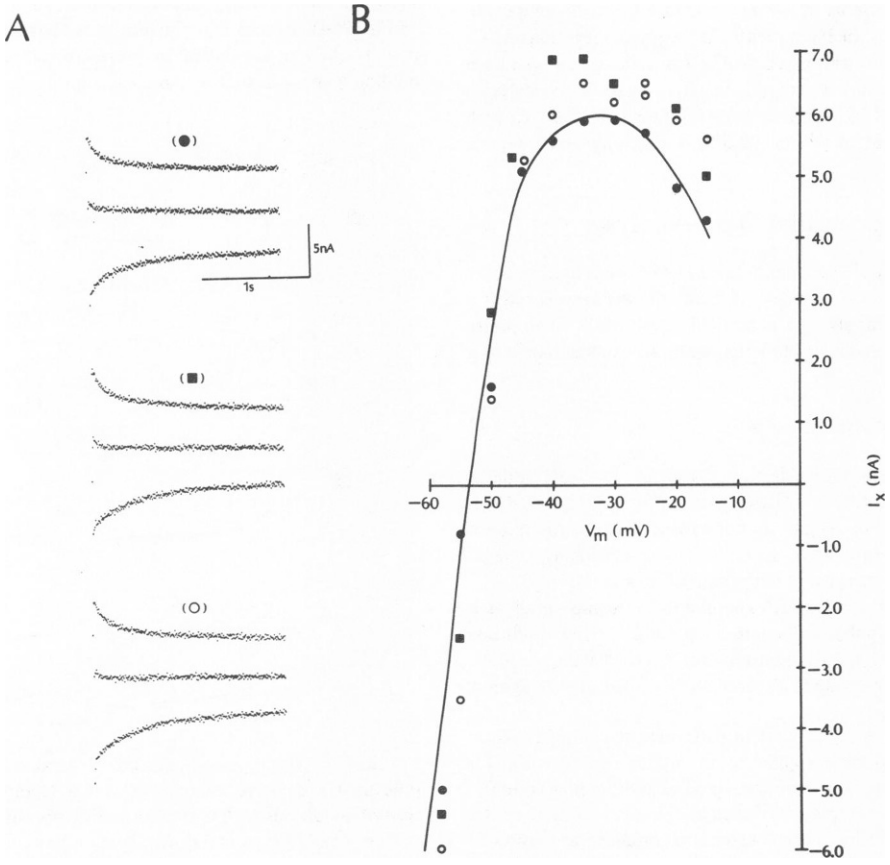

FIGURE 3 Prepulse duration and I_x reversal potential. (*A*) I_x tail currents recorded at voltages that bracket the reversal potential after 0.6 s (●), 1.5 s (■), and 3.0 s (○) prepulses to +10 mV. Return potentials (V_m) were −30, −50, and −58 mV for each case. (*B*) Zero-time amplitudes of I_x tails plotted against potential after prepulses of each duration (symbols as in *A*). Curve is hand-drawn through 0.6 s data. Holding potential was −30 mV. 16 mM K Tyrode's solution. Preparation AL.

preparations (Table I) and we found that shifts in I_x reversal potential were <5 mV with conditioning pulse durations of 3 s or less. This was true even for low (4 mM) potassium concentrations. As expected, sizeable shifts in the tail reversal potential could be induced by prolonged depolarization.

We also tested for changes in I_x reversal potential under conditions where the prepulse magnitude was varied at constant duration. In the experiment illustrated in Fig. 4, current tails reversed near −44 mV (Fig. 4 *A*) after 0.5 s prepulses to either +34 mV or +8 mV. Thus, the reversal potential of the I_x tail currents, measured after prepulses of either magnitude, was the same. These results and those from other similar experiments are included in Table I.

The absence of shifts in the I_x reversal potential indicates that changes in driving force due to ionic concentration changes in a restricted extracellular space do not significantly contribute to time-dependent changes in I_x, provided that activation prepulse duration is ≤3.5 s and that prepulse magnitude is ≤+35 mV.

This point is further supported by the findings that I_x kinetics and steady state activation are independent of external K concentration (see below). The remainder of the experiments presented in this paper used pulse protocols that do not produce accumulation or depletion. These protocols allow the measurement of reversal potentials over a 50-mV range, time constants and activation curves over an 80-mV range.

TABLE I
TESTS FOR ION ACCUMULATION IN EXTRACELLULAR SPACE

Expt.	$[K]_o$	Duration	Amplitude	V_{rev}	ΔV_{rev}
	mM	*s*	*mV*	*mV*	*mV*
CC‡	4	0.8	+25	−77	
		1.0	+25	−77	0
		1.5	+25	−75	2
		8	+25	−69	8
11-1	4	1.5	+10	−71	
			+20	−70	1
			+38	−75	−5
AA	8	0.5	+5	−65	
		1	+5	−65	0
		8	+5	−55	10
AL	16	0.6	+10	−53	
		1.5	+10	−53	0
		3	+10	−52	1
AM	12	0.5	+10	<−62	
		3.5	+10	−55	7
AN	12	1	+15	−55	
		3	+15	−55	0
AO	20	0.5	+10	−47	
		3.5	+10	−47	0
AS	20	0.5	+8	−45	
		3.5	+8	−45	0
BF	12	0.5	+13	−57	
		1	+13	−57	0
		3	+13	−56	1
AS	20	0.5	+8	−45	
		0.5	+34	−46	−1
AR*	20	0.5	+8	−45	
		0.5	+35	−43	2

*In the presence of 1 μM norepinephrine.
‡1 mM Cs

I_x is a Potassium Current

Figs. 3 and 4 have illustrated how I_x channel reversal potentials are obtained in 16 and 20 mM K_o solutions. Measurements with K_o below 10 mM are hampered by the presence of time-dependent pacemaker current, which is apparent at negative membrane potentials (Noble and Tsien, 1968; Hauswirth et al., 1972; DiFrancesco, 1981) as shown in Fig. 5 *A*. Clearly, outward I_x tails are apparent at potentials more depolarized than about −70 mV; at −75 mV pacemaker current makes a determination of the reversal potential difficult. The reversal potential can be estimated in this case, however, by extrapolating the instantaneous current-voltage relation for the I_x tails through the zero current axis as shown. A value of −73 mV is obtained. In two other experiments pacemaker currents were too large to accurately estimate the reversal potential in 4 mM K_o. However, outward current tails were seen at −70 mV, so V_{rev} was more negative than −70 mV.

A more direct method is to reduce the pacemaker current with external Cs (Isenberg, 1976). Such an experiment is illustrated in Fig. 5 *B*. While there remains some pacemaker current (apparent at −85 mV), it is sufficiently reduced to provide a reasonable measurement of V_{rev} of −77 mV. Unfortunately, external Cs also blocks I_x current (~50% in this experiment), and so cannot be used routinely. While lower concentrations would have less effect on I_x, the reduction of pacemaker current would also be less.

The I_x tail reversal potential data from 22 experiments are summarized in Fig. 6, which is a plot of the measured reversal potentials against extracellular potassium activity. The solid line is predicted by a constant field calculation (Goldman, 1943; Hodgkin and Katz, 1949), with internal activities of K and Na of 85.4 and 5.4 mM and P_{Na}/P_K = 0.02. These results demonstrate that this channel is very selective for potassium ions, selecting against Na by at least 50 to 1.

Potassium channels in several different cell types have complicated ion permeation properties. These properties are consistent with results expected from pores that can simultaneously be occupied by more than one ion (Hille and Schwarz, 1978; Begenisich and Smith, 1984). Under these conditions the constant field equation may not be appropriate. We use this equation here only to provide an estimate of relative Na, K permeability and to compare our

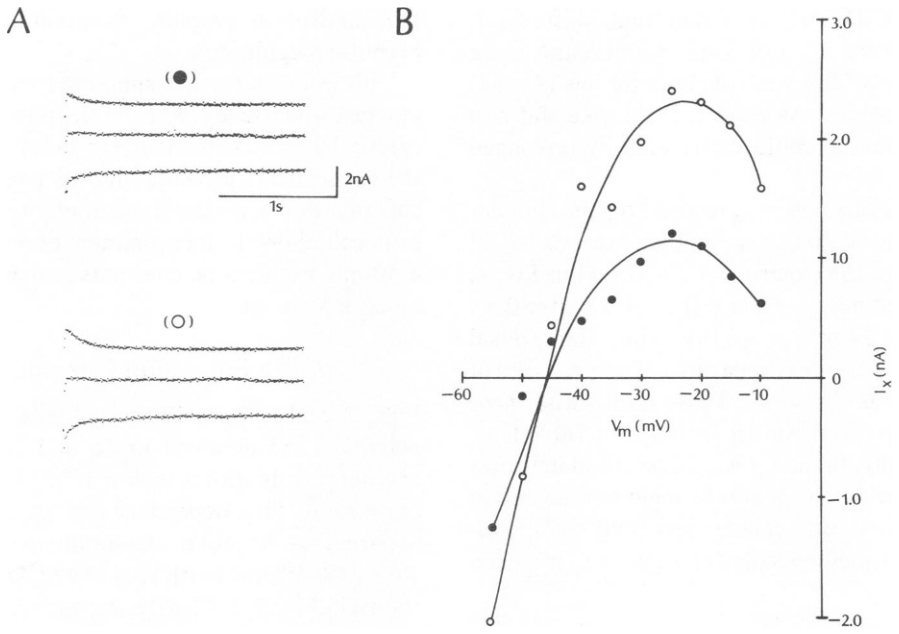

FIGURE 4 Influence of prepulse magnitude on I_x reversal potential. (*A*) I_x tail currents recorded near the I_x reversal potential after 0.5 s prepulses to +8 mV (●) and +34 mV (○). I_x tails are shown recorded at −20, −45, and −55 mV. (*B*) Zero-time amplitudes of I_x tails plotted against return potential (V_m) after prepulses to +8 mV and +34 mV (symbols as in *A*). The holding potential was −30 mV. 20 mM K Tyrode's solution. Preparation AS.

results to other potassium channels where the same equation has been used.

I_x Tail Relaxation is Biexponential

The time course of I_x tail relaxation was determined by fitting tail records with an equation containing two exponential terms (see Methods). An F-ratio test showed that the fit of two exponentials was statistically better ($P < .05$) than one exponential, but not significantly improved by the use of three exponentials. Deactivation of I_x was biexponential in all of our experiments.

Fig. 7 contains examples of tail currents recorded at several voltages along with the exponential function that yielded the best fit to each current record. Fitting exponentials to the current records in this manner allowed us to determine the voltage-dependence of the two time constants (τ_1 and τ_2) that describe I_x deactivation.

The results from many experiments designed to measure the time constants are summarized as filled symbols in Fig. 8. One time constant (τ_1) is relatively fast and increases with depolarization between −60 mV and −10 mV, and the second, slower time constant (τ_2) decreases with depolarization over the same voltage range. Most data points in this figure represent averages of 10–22 fibers. The smooth curves in the figure are the predictions of a model for the I_x channel described in Discussion.

Also shown in Fig. 8 are data from individual fibers in the presence of nisoldipine (△). These results demonstrate that the time constants are not distorted by the presence of calcium currents or transient outward currents.

We tested for, but did not find, systematic trends in time constants measured in different extracellular K concentrations. For example, at −40 mV the average value of τ_1 for all K_o was 62.9 ± 18 ms (±SEM, n = 16). At the same voltage, τ_1 was 64.3 ± 9.3 ms (n = 4) in 4 mM K_o, 54 ± 2.5 (n = 2) in 12 mM K_o, and 54 ± 3 ms (n = 3) in 16 mM K_o. At −15 mV, τ_1 was 114 ± 7.5 ms (n = 16) averaged over all K_o. At this voltage, τ_1 was 99 ± 16 ms (n = 5) in 4 mM K_o; 110 ± 19 ms (n = 2) in 12 mM K_o, and 119 ± 22 ms (n = 3) in 16 mM K_o. Similar results were obtained for τ_2.

It has been suggested (Attwell et al., 1979) that a biexponential tail current may be an artifact due to potassium concentration changes in a restricted space. If this were the case, then the measured time constants would be expected to be a function of the concentration of external potassium. The fact that we did not observe such a dependence supports the conclusion, obtained from loading tests, that our experiments are free of such artifacts.

I_x Activation Time Course at Positive Potentials is Apparently Monoexponential

At potentials more positive than about −10 mV, tails were relatively small because of the rectifying properties of the channel. Therefore, a second voltage protocol was used to study the time course of I_x activation at more positive potentials. In this case constant test pulse amplitudes of increasing duration were used. The envelope of tail currents measured at the holding potential after each test pulse reflects the time course of I_x activation that occurs at the test voltage (Noble and Tsien, 1969).

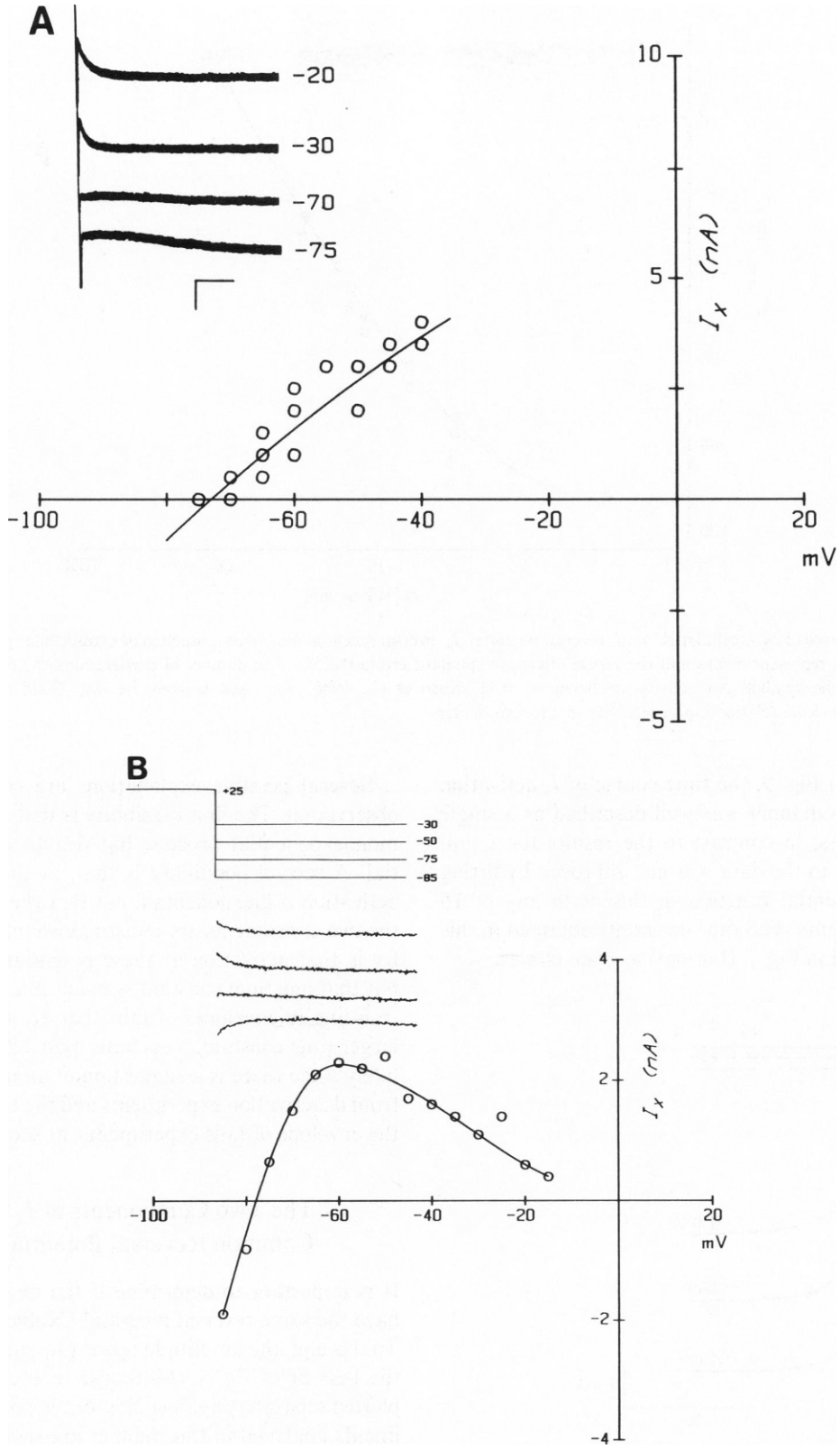

FIGURE 5 (*A*) Estimation of the I_x reversal potential in 4 mM $[K]_o$. *Inset:* I_x tails measured at −20, −30, −70, and −75 mV following a 1-s pulse to +38 mV. Currents measured at −70 and −75 are contaminated by pacemaker currents. Calibration bars: 5 nA, 0.5 s. Graph: Current-voltage relationship of tail magnitudes obtained with prepulses to either +10 or +20 mV. The extrapolated reversal potential was −73 mV. (*B*) Cs as a tool to block pacemaker currents. *Inset:* I_x tails measured in 4 mM $[K]_o$ and 1 mM $CsCl_2$. (0.8 s pulse to +25 mV followed by potentials indicated.) Voltage protocol is shown above current traces. The presence of 1 mM $CsCl_2$ sufficiently blocked pacemaker currents to allow a clear estimate of the I_x reversal potential in 4 mM K_o. Note that there is still a time dependent component in the current trace at −85 mV, characteristic of the presence of the pacemaker current. This Cs concentration reduced the magnitude of the I_x tails by 50%. Graph: Current-voltage relationship of I_x in the presence of 1 mM $CsCl_2$. The reversal potential was −77 mV.

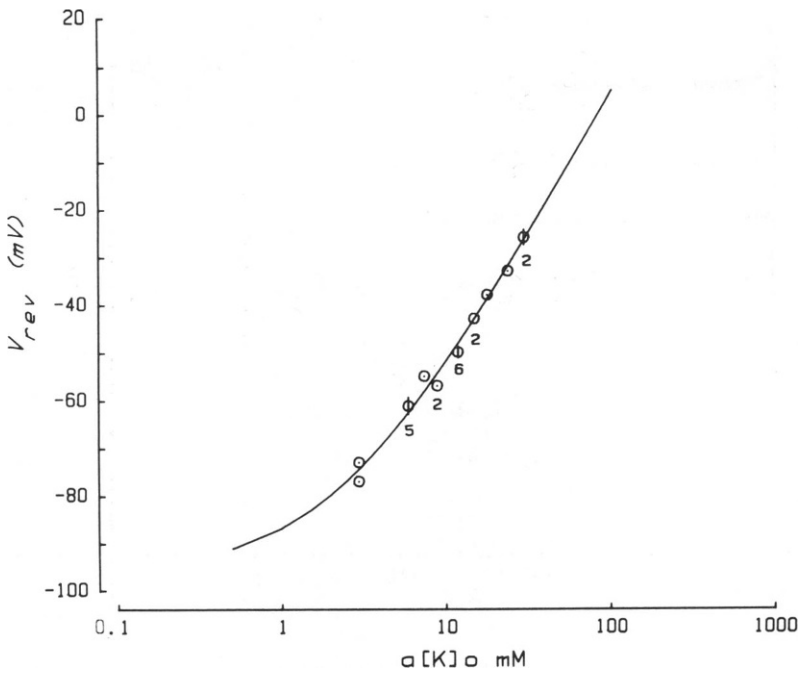

FIGURE 6 Influence of extracellular K^+ on I_x reversal potential. I_x reversal potential plotted as a function of extracellular potassium activity (aK_o). The circles represent means and the vertical bars are standard errors (SEM). The number of preparations, if greater than one, is indicated below the symbol. An activity coefficient of 0.73 (Sheu et al., 1980) was used to compute aK_o. Solid curve: best fit of Goldman-Hodgkin-Katz relationship to data. See text for parameters.

As illustrated in Fig. 9, the time course of I_x activation determined in this manner was well-described as a single exponential process, in contrast to the results for I_x tail relaxation. The fit to the data was not improved by fitting with a two-exponential function in this or in any of 16 similar measurements. The time constants obtained in this fashion are plotted in Fig. 8 (bottom) as open circles.

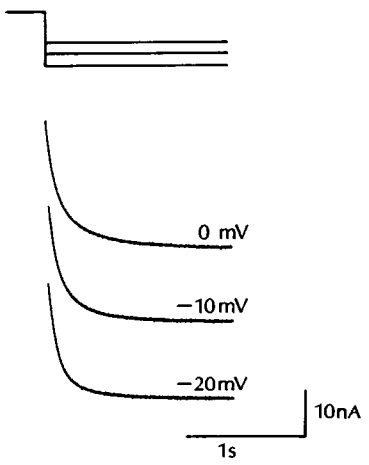

FIGURE 7 Time course of I_x tail relaxation. Family of current tails recorded after 0.8 s prepulses to +26 mV at the following return potentials (indicated in figure): 0, −10, and −20 mV. The solid curve superimposed on each trace is the best fit of Eq. 1 to the data. The time constants (ms) obtained from the procedure are: 0 mV: τ_1 = 83, τ_2 = 401; −10 mV: τ_1 = 83, τ_2 = 350; −20 mV: τ_1 = 77, τ_2 = 374 ms. Holding potential was −30 mV. 4 mM K_o Tyrode's; Preparation AV.

Several possible explanations are consistent with this observation. The first possibility is that activation of I_x is a monoexponential process, but deactivation is biexponential. A second possibility is that, at the voltages studied, activation is biexponential, but that the time constants for the two components are indistinguishable. A third possibility is that activation at these potentials is biexponential, but that one time constant is much smaller than the other, resulting in envelopes of tails that are fitted by the single larger time constant. This latter possibility seems the most likely since there is a suggestion of an overlap of τ_2 values from deactivation experiments and the time constants from the envelope of tails experiments, as seen in Fig. 8.

The Two Components of I_x Share a Common Reversal Potential

It is important to determine if the two components of I_x have the same reversal potential (Noble and Tsien, 1969). To this end, the amplitude terms (A_1 and A_2) that provided the best fit of Eq. 1 (Methods) to each tail record were plotted separately against membrane potential. Two experiments analyzed in this manner are shown in Fig. 10. The reversal potentials of the two components in Fig. 10 *A* are −50.6 and −50.4 mV, and are −46.3 and −45.5 mV in Fig. 10 *B*. From nine measurements on six preparations, an average difference between the reversal potentials of the two components was found to be 2.3 ± 0.8 mV. Of these, all but two values were <3 mV.

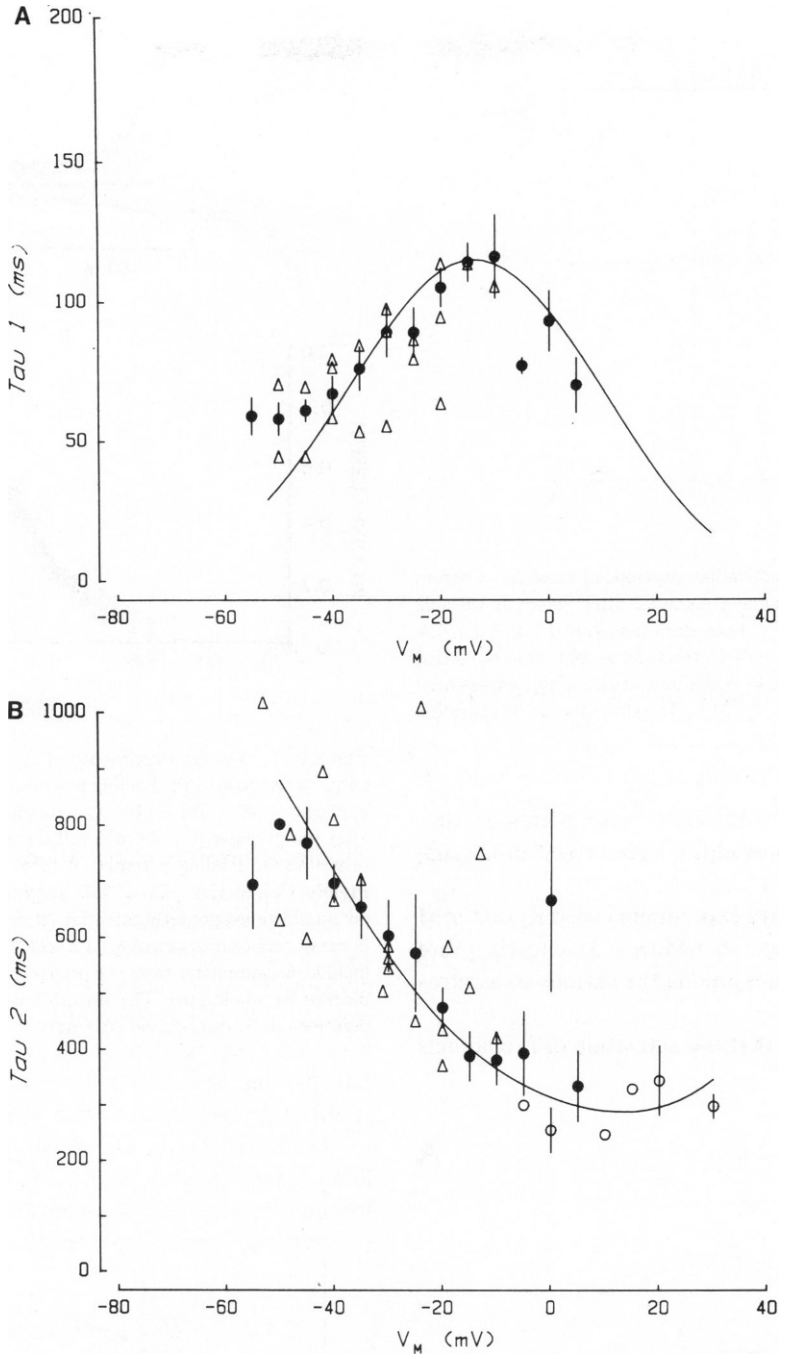

FIGURE 8 Voltage-dependence of I_x time constants. Time constants determined by fitting Eq. 1 to I_x tails (●), or by fitting single time constant functions to envelopes of I_x tails (○). Data are shown as mean ± SEM. Points without standard errors represent a single measurement or the SEM was smaller than the symbol. The triangles indicate time constants of tail currents measured in the presence of nisoldipine. Smooth curves are determined by the model described in Discussion.

Since the two components of I_x tail current appear to have a common reversal potential under the conditions of these experiments, there is no need to interpret these data as current through two separate pathways. Instead, our data are consistent with the notion that I_x is carried by one population of channels that can exist in more than two states. This interpretation is used in the remainder of this paper.

I_x Activation Occurs Over a Broad Range of Potentials

The voltage-dependence of the activation of I_x is shown in Fig. 11. The activation curve for each fiber was obtained by plotting I_x tail magnitudes as a function of prepulse potential. Measurements from 21 preparations were scaled (not shifted) as described in the Appendix and are plotted

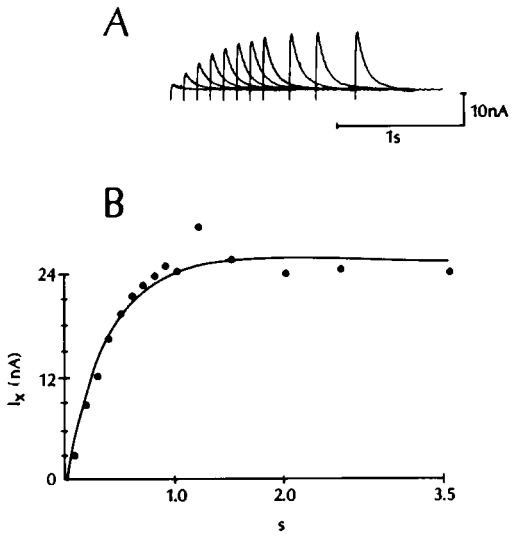

FIGURE 9 Time course of I_x activation: envelope of tails. (A) Current tails recorded at a −30-mV holding potential after pulses of variable duration were applied to +30 mV. Pulse durations were 0.1, 0.2, 0.3, 0.4, 0.5, 0.7, 0.8, 1.0, 1.2, and 1.5 s. (B) Current tail amplitudes are plotted against pulse duration. Solid curve is the best fit of a single exponential function to the data. τ = 363 ms. 4 mM K_o Tyrode's solution. Preparation 13.2.

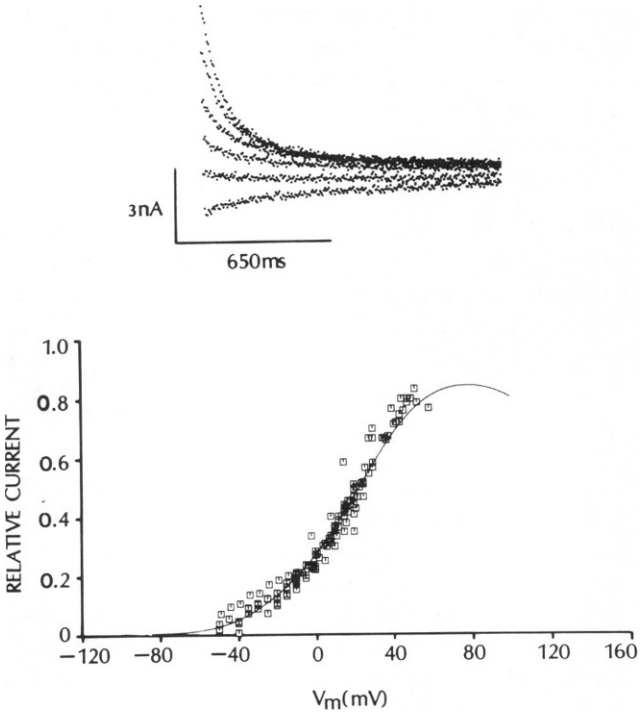

FIGURE 11 Voltage-dependence of I_x activation. *Inset:* Family of tail currents recorded at the holding potential (−34 mV) after prepulses were applied to −49, −29, −14, +1, +16, and +26 mV. The I_x tail, recorded after the prepulse to −49 mV, reflects an increasing I_x conductance on return to the holding potential. 4 mM K Tyrode's solution. Fiber AI. *Figure:* Cumulative plot of tail amplitudes measured at the holding potential against prepulse potential. Measurements, from 21 preparations in various concentrations of K_o, are scaled for comparison. These data also include measurements from five preparations with Ca-dependent currents blocked by nisoldipine. The smooth curve is determined by the model described in Discussion and Appendix.

in this figure. The curve through these points is that predicted by the kinetic model for I_x described in Discussion and Appendix.

Included in this figure are experiments with K_o of 4 mM (n = 14), 8 mM (n = 4), and 16 mM (n = 3). Clearly, there are no significant differences among the various concentrations.

It is clear from Fig. 11 that the activation of I_x channels

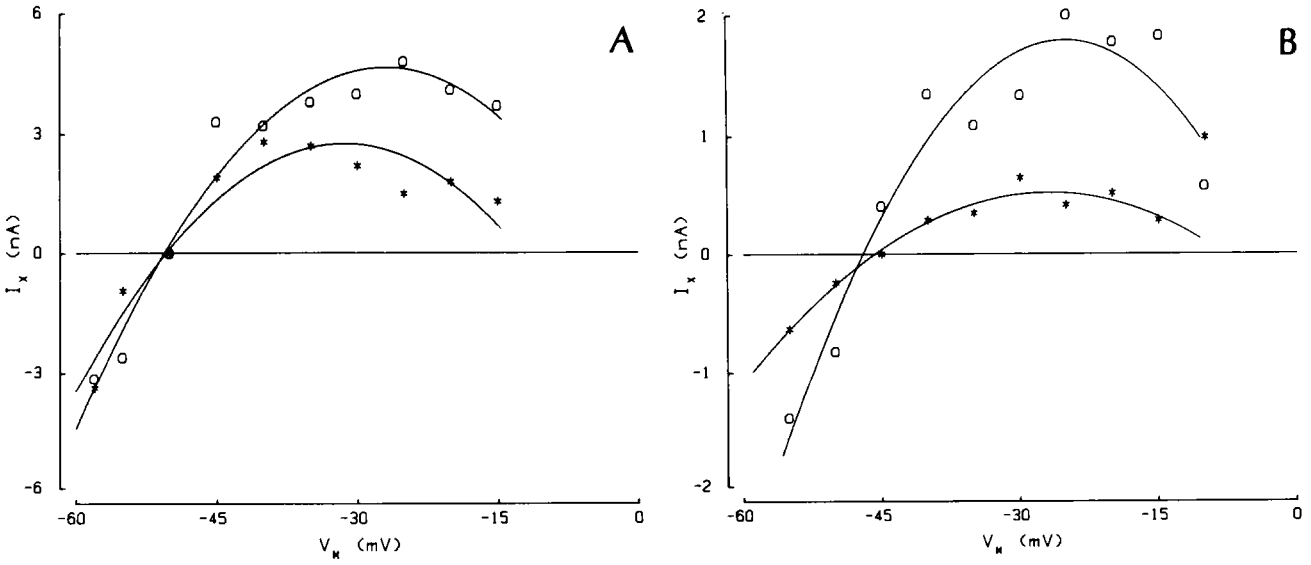

FIGURE 10 Two amplitude components of I_x as functions of membrane potential. I_x tails were recorded at a series of potentials after prepulses to a common pulse voltage and analyzed as described in the text. The fitted amplitudes of the two exponential terms are plotted against membrane potential (V_m). The smooth curves are quadratic functions of voltage fitted to the data. (A) 16 mM K Tyrode's solution. Preparation AL. (B) 20 mM K Tyrode's solution. Preparation AS.

occurs over a broad voltage range. Activation may not be complete even at potentials as positive as +40 mV. As discussed later, this appears to be a common property of many types of potassium channels.

DISCUSSION

An important result of this study is the finding that delayed rectification in the calf Purkinje fiber can be quantitatively studied without complications from accumulation or depletion of charge carrier. Evidence for this point is provided by the invariance of the I_x reversal potential when prepulses are kept within the limits suggested by Table I: durations of 3.5 s or less, magnitudes of +35 mV or less. The fact that I_x deactivation was biexponential when prepulses were kept within this range demonstrates that the slower time-dependent changes in I_x are due not to changes in ion concentration, but to intrinsic properties of the I_x channels. Our observation that the I_x time constants are functions of membrane potential, but are independent of extracellular potassium concentration, further supports this conclusion. Furthermore, because we find that the two components share a common reversal potential, there is no reason to suppose that I_x is carried by two populations of channels. Although we cannot rule out the existence of two types of I_x channels, our data are consistent with the simpler situation of one population of channels with multiple state kinetics.

The most complete previous investigation of delayed rectification in the cardiac Purkinje fiber is the work of Noble and Tsien (1969) using fibers obtained from sheep hearts. Noble and Tsien observed two exponential components of I_x tail relaxation in their preparations, but in contrast to the present results, they found a sizeable (20 mV) difference between the reversal potential of these two components. They also observed differences between the rectifier properties of the two components. I_{x1} was an inward rectifier, but I_{x2} did not rectify. Because of the differences in reversal potential and voltage-dependence, Noble and Tsien (1969) interpreted their data as current through two independent pathways (I_{x1} and I_{x2}).

Unfortunately, a quantitative comparison of our results to those of Noble and Tsien (1969) is complicated by the differences in experimental conditions and biological preparations (sheep and calf). Of particular concern are the extremely long duration (10–20 s) voltage steps used by Noble and Tsien, since it has been suggested that such voltage protocols can promote extracellular potassium accumulation (McGuigan, 1974; Noble, 1976; McDonald and Trautwein, 1978).

Selectivity

The presence of time-dependent currents at voltages negative to −65 mV complicates the measurement of I_x tail current in this voltage range (Noble and Tsien, 1968; Hauswirth et al., 1972; DiFrancesco, 1981). Consequently, the P_{Na}/P_K ratio of 0.02 described above is, if anything, an overestimate. The I_x pore may be even more K selective.

Noble and Tsien (1969) suggested that I_{x1} is carried largely, but not exclusively, by K^+ ions after measuring V_{rev} for I_{x1} in one K concentration and in a limited number of experiments. We find that I_x channels are very selective for K^+ ions. In fact, the selectivity of I_x channels resembles that of other delayed rectifier K^+ channels. Relative permeabilities, determined for delayed rectifier channels in squid axons (Bezanilla and Armstrong, 1972), myelinated nerve (Hille, 1975), and snail neurons (Reuter and Stevens, 1980) indicate a range of P_{Na}/P_K ratios of 0.01 to 0.07 (reviewed by Latorre and Miller, 1983); our estimate for P_{Na}/P_K of 0.02 is within this range.

Potassium Channel Activation

The activation curve for I_x channels shown in Fig. 11 extends to large potentials. Indeed, we found no clear saturation up to the largest potentials used in this study (40 mV). The lack of saturation is not an ionic accumulation artifact since larger depolarizations would increase external potassium and reduce outward currents. Also, we find no differences among activation curves obtained over a 10-fold range of external potassium.

The broad range of activation seen in Fig. 11 is not restricted to Purkinje fibers or multicellular preparations. We have observed very similar results in isolated guinea pig myocytes. Beam and Donaldson (1983*a*) measured potassium conductance in rat skeletal muscle using the three-microelectrode technique and found saturation only at large potentials. The potassium conductance of squid giant axons saturates at potentials above 80 mV (Gilly and Armstrong, 1982). Thus, this property appears to be a rather general property of delayed rectifier potassium channels.

A Kinetic Model

These data suggest that I_x is carried by one population of channels. Since the relaxation of this current is biexponential, the kinetics of these channels cannot be explained by first order models. A model of the Hodgkin-Huxley "n^2" type predicts two exponential components with time constants differing by a constant factor of two. The data plotted in Fig. 8 show such a model cannot accurately describe I_x channel current, since the ratio of time constants is clearly not the same at all potentials.

The kinetic scheme must be more complex: the channel must be able to exist in at least three states. The simplest three state scheme would include two nonconducting (closed) states coupled sequentially to a third conducting (open) state:

$$C \underset{k_{21}}{\overset{k_{12}}{\rightleftharpoons}} C \underset{k_{32}}{\overset{k_{23}}{\rightleftharpoons}} O.$$

In this simplest case, channel conductance is proportional

to the probability of being in the open state. Such a scheme is completely characterized by the rate constants that govern transitions between states.

More complicated kinetic schemes can be imagined in which the open state is coupled to the first closed state in a cyclic fashion or a model with multiple conducting states. However, we find that the simpler model quantitatively accounts for our experimental observations and therefore, there is no need to consider more complex schemes.

In fact, all of our kinetic observations can be described in terms of the four voltage dependent rate constants, derived directly from the experimental data by procedures described in the Appendix. The voltage dependence of I_x channel time constants (Fig. 8) and steady state activation data (Fig. 11) are reproduced using these rate constants.

The voltage dependence of the system time constants that results from these rate constants explains our observation that the relaxation of I_x tails were biexponential, whereas envelope of tails experiments (see Methods) appeared to be monoexponential. From Fig. 8 it is apparent that in the case of envelope of tails experiments, the first exponential process (characterized by τ_1) would be too fast to be resolved at potentials more positive than +10 mV.

Plots of the logarithms of the four rate constants are shown in Fig. 12. The solid lines represent quadratic functions of voltage with the specific parameter values given in the figure legend. Our experimentally derived rate constants, therefore, can be approximated by the following equation:

$$k_{ij} = \exp(A + B \cdot V + C \cdot V^2). \quad (2)$$

As described by Stevens (1978), such a voltage dependence is expected from energetic considerations of the conformational states of a membrane-bound macromolecule in an electric field.

The functional relationship between the rate constants and membrane potential contains information about the attempt rate for crossing the energy barriers between conformations, the free energy differences between conformations, and the contributions of dipoles, induced dipoles, and other charges that experience a fraction of the transmembrane electrical field. The first term (A) of the equation is related to the energy of the system in the absence of an applied electric field, including bond strain and hydrophobic interactions. The higher order terms

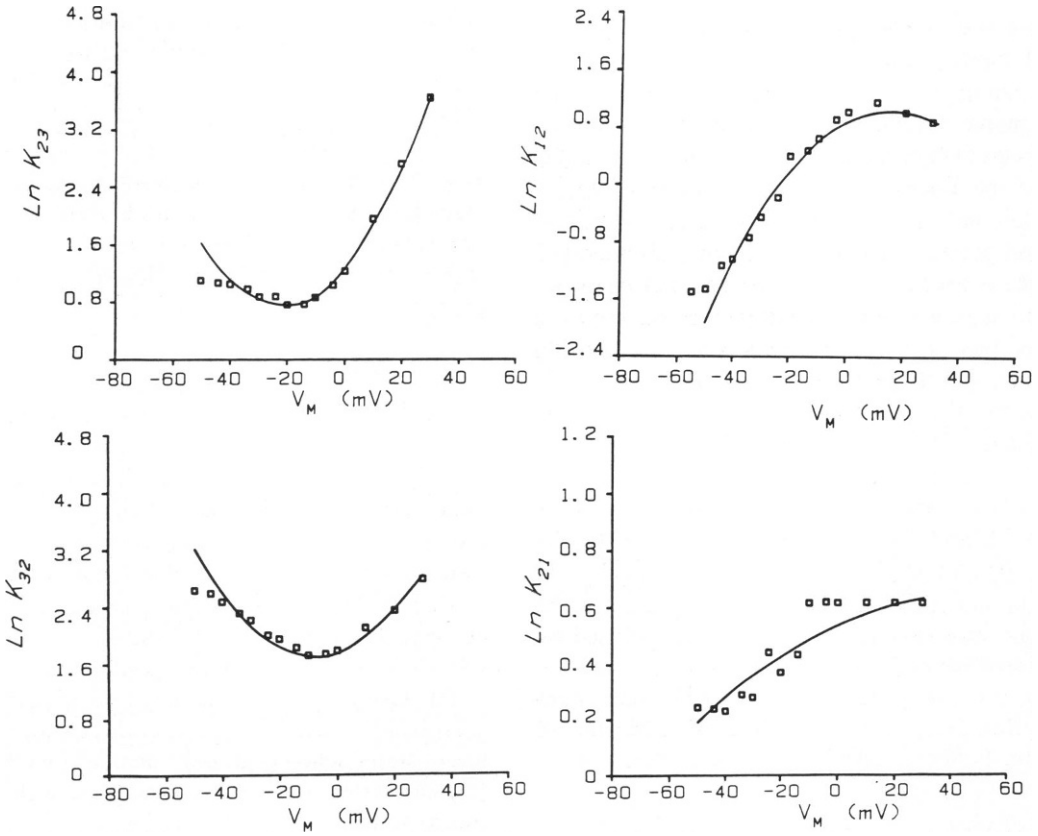

FIGURE 12 Voltage dependence of rate constants. The natural logarithm of the four rate constants (k_{12}, k_{21}, k_{23}, and k_{32}) (derived from the data as described in the Appendix) are plotted as a function of membrane potential (V_m). See sequential three-state model in *A Kinetic Model* and in the Appendix. The solid curve in each panel is a quadradic function of voltage of the form: $\ln k_{ij} = A + BV + CV^2$. The free parameters ($A$, B, and C) were adjusted to give the fit shown in each case. k_{32}: $A = 1.77$, $B = 0.0117$, $C = 8.07 \times 10^{-4}$; k_{21}: $A = 0.536$, $B = 0.00453$, $C = -4.73 \times 10^{-5}$; k_{23}: $A = 1.26$, $B = 0.048$, $C = 1.11 \times 10^{-3}$; k_{12}: $A = 0.900$, $B = 0.0208$, $C = -7.2 \times 10^{-4}$. Units: B (mV^{-1}); C (mV^{-2}).

(B and C) are important when an electric field is imposed. In particular, a linear dependence on voltage arises from dipole-field interactions, whereas a quadratic dependency may result from the effects of field-induced dipoles.

The voltage dependence of our rate constants suggest that induced dipoles are important in the gating of the I_x channel. It is possible to compute from our rate constants the change in the component of the electric dipole moments in the direction of the electric field that occurs when the channel changes state. These calculations are beyond the scope of the present work and will be described in the future.

It is often implicitly assumed, when modeling channel kinetics, that membrane depolarization monotonically increases forward (toward the open state) and decreases backward rate constants. Our results suggest this may not (and need not) be the case. All that is necessary is that the voltage dependence of the rate constants be such that depolarization increases the probability of finding channels in the open state. This certainly occurs in the present work but even at large depolarizations not all the channels are open. This result is seen in Fig. 11 as values of relative activation of less than unity.

Although we can account for all of our kinetic observations with the rate constants presented, it is not possible to obtain from these measurements estimates of single channel conductance and the number of channels; nor, in general, can gating mechanisms be uniquely defined entirely on kinetic arguments. However, our approach allows us to place constraints on possible gating schemes. We can definitely rule out a kinetic model of the Hodgkin and Huxley type; whereas, a second-order model was in good agreement with the results. We cannot, of course, eliminate still higher order models with many similar time constants such that only two could be resolved. An analysis of current fluctuations and the direct measurements of single channel properties may allow us to more completely define the I_x channel on a molecular level.

APPENDIX

As pointed out in Results, the data require a second-order kinetic model to describe the gating of I_x channel currents. Our goal was to see if a relatively simple second-order model could account for these results. To use a three-state model to describe the time courses of ionic currents, it is necessary to solve a second-order differential equation or a system of coupled first-order differential equations that define the model. Possible three-state models include the following configurations:

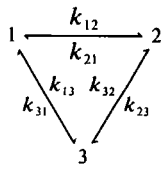

$$1 \underset{k_{21}}{\overset{k_{12}}{\rightleftharpoons}} 2 \underset{k_{32}}{\overset{k_{23}}{\rightleftharpoons}} 3 .$$

In the most general model, all possible transitions between states are allowed. Simpler state diagrams result if it is known that certain transitions are not allowed. In such cases, some of the rate constants are equal to zero. In the absence of a priori knowledge of the manner in which the states interact it is usually necessary to arbitrarily choose a given configuration and try to obtain rate constants consistent with the experimental observations. If a given model can not be made to fit, another is chosen and the system equations must be solved again. To analytically solve the system equations it is often necessary to make simplifying assumptions. Once the model is solved using these assumptions, its use is only valid if the assumptions are reasonably fulfilled. To circumvent these difficulties we have turned to numerical methods to produce a general solution to the system equations. Using this technique, one is free to easily change model configurations simply by adding or removing particular rate constants. The solutions are not dependent upon arbitrary assumptions.

We have fitted our data with the constrained three-state system shown above using a computer program that numerically integrates the system equations and searches for the best fitting estimates of the rate constants. These rate constants can then be used to calculate the time course of state occupancy and the fractional occupancy at steady state.

The model rate constants were obtained from our data using a general method for least squares estimation of nonlinear parameters (Marquardt, 1963). The method involves searching a parameter space for a set of parameters (the rate constants in this case) that results in the smallest sum of the squared differences between the model equation(s) and the data. The search procedure automatically alternates between the method of steepest descent and a Gauss-Newton type linearization, depending on proximity to a minimum on the SUM OF SQUARES hypersurface. The fitting procedure was implemented as a FORTRAN program and the function to be fitted to the data was contained in a subroutine (Bevington, 1969). When fitting a differential equation model to the data, the function subroutine contained the system of first-order differential equations for the desired model. During each call to this subroutine, the system of equations was numerically integrated. The integrated solution was then compared to the data. The fitting program adjusts the rate constants and calls the integration routine for another solution. This was repeated until the best fitting values of the rate constants were obtained.

For integrating the system of first-order differential equations we used a fourth-order Runge-Kutta method as modified by Gill (see Ralston and Wilf, 1960). This is a single-step method that automatically adjusts the integration step size. Accuracy is tested by comparing the results from halving the step size. The step size reduction can be repeated as many times as necessary to achieve the desired degree of accuracy.

The general equations that describe the behavior of a channel with n conformational states can be expressed as

$$\frac{dP_i}{dt} = -\sum_{j=1}^{n} k_{ij}P_i(t) + \sum_{j \neq i} k_{ji}P_j(t), \qquad \begin{matrix} i = 1, 2, \ldots n \\ j \neq i \end{matrix} \tag{A1}$$

where P_i is the probability that the channel is in state i and k_{ij} is the transition rate from state i to state j. We have placed the following constraints on the general model

$$n = 3 \tag{A2}$$

$$P_1(t) + P_2(t) + P_3(t) = 1 \tag{A3}$$

$$k_{13} = k_{31} = 0 \tag{A4}$$

and we find that our data are best represented by assuming a single conducting state. These constraints result in the following channel diagram that was fitted to our data:

$$\mathrm{C} \underset{k_{21}}{\overset{k_{12}}{\rightleftharpoons}} \mathrm{C} \underset{k_{32}}{\overset{k_{23}}{\rightleftharpoons}} \mathrm{O} .$$

It often was difficult, experimentally, to inject enough current with microelectrodes to voltage clamp the membrane to the extreme positive potentials ($>+60$ mV) required to fully activate I_x. Therefore, we

estimated the steady state occupancy of P_3 by fitting the steady state activation data with the following empirical equation:

$$I(V) = I\max/\{1 + \exp[(B - V)/C]\}, \quad \text{(A5)}$$

where Imax is the plateau achieved at extreme positive voltages, V is membrane potential, and B and C are constants related to the half maximal value and the slope of $I(V)$, respectively. The best fit of Eq. A5 to the activation data allowed an estimate of Imax. The fitted value of Imax was used to normalize the activation data into a range from 0 to 1.

The parameters of Eq. 1 (Methods), A_1 and A_2, were normalized to be fractions (A_1' and A_2') of the maximum current at any potential. The values, A_1' and A_2', were then used with the time constants (τ_1 and τ_2) and the activation data, $P_3(\infty)$, to generate the time course of occupancy in the conducting state:

$$P_3(t) = A_1' \cdot \exp(-t/\tau_1) + A_2' \cdot \exp(-t/\tau_2) + P_3(\infty). \quad \text{(A6)}$$

The model equations were then fitted to these experimentally determined values to obtain best least squares estimates of the rate constants at each membrane potential.

For this particular case of a closed, sequential three-state system, the system time constants are given by the following equations:

$$1/\tau_1 = 0.5 \cdot [C_2 + (C_2^2 - 4C_1)]^{1/2} \quad \text{(A7)}$$

$$1/\tau_2 = 0.5 \cdot [C_2 - (C_2^2 - 4C_1)]^{1/2}, \quad \text{(A8)}$$

where $C_1 = k_{21} \cdot k_{32} + k_{12} \cdot k_{23} + k_{32} \cdot k_{12}$, and $C_2 = k_{12} + k_{21} + k_{32} + k_{23}$. At steady state, $\dot{P}1 = \dot{P}2 = \dot{P}3 = 0$, therefore Eq. A1 can be solved for P_3:

$$P_3(\infty) = k_{12} \cdot k_{23}/C_1. \quad \text{(A9)}$$

The steady state occupancies of state 2 and state 3 are similarly given by:

$$P_2(\infty) = k_{12} \cdot k_{32}/C_1 \quad \text{(A10)}$$

$$P_1(\infty) = k_{32} \cdot k_{21}/C_1, \quad \text{(A11)}$$

where the numerators in all three equations are the product of the two rate constants pointing toward the appropriate state. Eqs. A7–A9 are used to compute system time constants and steady state fractional occupancy of the conducting state from the derived rate constants.

At membrane potentials more positive than −10 mV, it was difficult to measure the time course of relaxing tail currents due to rectification; beyond +5 mV, measurement of tail currents was usually not possible. Therefore, an envelope of tails protocol was used to obtain kinetic information at potentials more positive than 0 mV. The time course of activation at these positive potentials was always characterized as a single exponential process. This finding could have several explanations (see Results). Rather than make any assumptions about the fact that the kinetics were biexponential at negative membrane potentials, but appeared monoexponential at potentials more positive than 0 mV, the rate constants at positive membrane potentials were estimated as follows. The rate constants obtained from relaxing tail currents (−50 to −10 mV) were plotted and extrapolated to membrane potentials more positive than −10 mV. The extrapolated values of rate constants were adjusted until they could reproduce the measured time constants and $P_3(\infty)$ at potentials from 0 to 30 mV. The rate constants at each potential from −50 to +30 mV were then fitted with Eq. 2 (see Discussion) which was used to calculate the predicted voltage dependence of the rate constants (smooth curves in Fig. 12). The predicted voltage dependences from Eq. 2 were used with Eqs. A7–A9 to predict the voltage dependence of the system time constants and activation data (smooth curves in Figs. 8 and 11, respectively).

We gratefully acknowledge the assistance of John Young for the electronic instrumentation, Susan Kass for the art work, and Karen Vogt and Margot Hattler for secretarial assistance.

Financial support was provided by National Science Foundation grant PCM-8116822 to Ted Begenisich and Robert S. Kass and by a National Institutes of Health Postdoctoral Fellowship to Leslie C. McKinney.

Received for publication 18 February 1985 and in final form 29 May 1985.

REFERENCES

Allen, D. G., D. A. Eisner, and C. H. Orchard. 1984. Characterization of oscillations of intracellular calcium concentrations in ferrent ventricular muscle. *J. Physiol. (Lond.).* 352:113–128.

Attwell, D., D. Eisner, and I. Cohen. 1979. Voltage-clamp and tracer flux data: effects of a restricted extracellular space. *Q. Rev. Biophys.* 12:213–261.

Beam, K. G., and P. L. Donaldson. 1983*a*. A quantitative study of potassium channel kinetics in rat skeletal muscle from 1 to 37°. *J. Gen. Physiol.* 81:485–512.

Beam, K. G., and P. L. Donaldson. 1983*b*. Slow components of potassium tail currents in rat skeletal muscle. *J. Gen. Physiol.* 81:513–530.

Begenisich, T., and C. Smith. 1984. Multi-ion nature of potassium channels in squid axons. *Curr. Top. Membr. Transp.* 22:353–369.

Bennett, P. B., L. C. McKinney, R. S. Kass, and T. B. Begenisich. 1984. Delayed rectification in the calf cardiac Purkinje fiber: evidence for multiple state kinetics. *Biophys. J.* 45(2, Pt. 2):137*a* (Abstr.)

Bevington, P. R. 1969. Data Reduction and Error Analysis for the Physical Sciences. McGraw-Hill Book Co., New York. 336 pp.

Bezanilla, F., and C. M. Armstrong. 1972. Negative conductance caused by entry of sodium and cesium ions into the potassium channels of squid axons. *J. Gen. Physiol.* 60:588–608.

Brown, H. F., and S. J. Noble. 1969. Membrane currents underlying delayed rectification and pacemaker activity in frog atrial muscle. *J. Physiol. (Lond.).* 204:717–736.

Colatsky, T. J. 1980. Voltage clamp measurements of sodium channel properties in rabbit cardiac Purkinje fibres. *J. Physiol. (Lond.).* 305:215–234.

Colquhoun, D., E. Neher, H. Reuter, and C. F. Stevens. 1981. Inward current channels activated by intracellular calcium in cultured cardiac cells. *Nature (Lond.).* 294:752–754.

Dani, A. M., A. Cittadini, and G. Insei. 1979. Calcium transport and contractile activity in dissociated mammalian heart cells. *Am. J. Physiol.* 237:C147–C155.

DiFrancesco, D. 1981. A new interpretation of the pacemaker current I_{K2} in Purkinje fibres. *J. Physiol. (Lond.).* 314:359–376.

Fozzard, H. A., and M. Hiraoka. 1973. The positive dynamic current and its inactivation properties in cardiac Purkinje fibres. *J. Physiol. (Lond.).* 234:569–586.

Gilley, W. F., and C. M. Armstrong. 1982. Divalent cations and the activation kinetics of potassium channels in squid giant axons. *J. Gen. Physiol.* 79:965–996.

Goldman, D. E. 1943. Potential, impedance, and rectification in membranes. *J. Gen. Physiol.* 27:37–60.

Green, W., J. Goto, and T. J. Colatsky. 1983. Ionic basis for delayed rectification in cardiac Purkinje fibers. *Biophys. J.* 41(2, Pt. 2):74*a*. (Abstr.)

Hauswirth, O., D. Noble, and R. W. Tsien. 1972. Separation of the pacemaker and plateau components of delayed rectification in cardiac Purkinje fibres. *J. Physiol. (Lond.).* 225:211–235.

Hille, B. 1975. Ionic selectivity of Na and K channels of nerve membranes. *In* Membranes, vol. 3. G. Eisenman, Editor. Marcel Dekker, Inc., New York. 255–323.

Hille, B., and W. Schwarz. 1978. Potassium channels as multi-ion single-file pores. *J. Gen. Physiol.* 72:409–442.

Hodgkin, A. L., and B. Katz. 1949. The effect of sodium on the electrical activity of the giant axon of the squid. *J. Physiol (Lond.)*. 108:37–77.

Hume, J. R. 1983. Time-dependent outward current in isolated guinea pig atrial and ventricular myocytes. *Biophys. J.* 41(2, Pt. 2):74*a* (Abstr.)

Isenberg, G. 1976. Cardiac Purkinje fibers: cesium as a tool to block inward rectifying potassium currents. *Pfluegers Arch. Eur. J. Physiol.* 365:99–106.

Isenberg, G., and U. Klockner. 1982*a*. Calcium currents of isolated bovine ventricular myocytes are fast and of large amplitude. *Pfluegers Arch. Eur. J. Physiol.* 395:30–41.

Isenberg, G., and U. Klockner. 1982*b*. Calcium tolerant ventricular myocytes prepared by preincubation in a "KB medium." *Pfluegers Arch. Eur. J. Physiol.* 395:6–18.

Jaeger, J. M., and W. R. Gibbons. 1981. The effect of 4-aminopyridine on the late outward plateau currents in cardiac Purinje fibers. *Biophys. J.* 33(2, Pt. 2):72*a*. (Abstr.)

Kass, R. S. 1982. Nisoldipine: a new more selective Ca current blocker in calf Purkinje fibers. *J. Pharmacol. Exp. Ther.* 223:446–456.

Kass, R. S. 1984. Delayed rectification is not a Ca-activated current in the calf Purkinje fiber. *Biophys. J.* 45:837–839.

Kass, R. S., and P. B. Bennett. 1985. Microelectrode voltage clamp: the cardiac Purkinje fiber. *In* Voltage and Patch Clamping with Microelectrodes. T. G. Smith, H. Lecar, S. Redman, and P. Gage, editors. Waverly Press, Baltimore. 178–191.

Kass, R. S., and M. C. Sanguinetti. 1984. Calcium channel inactivation in the calf cardiac Purkinje fiber: evidence for voltage dependent and Ca-mediated inactivation. *J. Gen. Physiol.* 84:706–726.

Kass, R. S., S. A. Siegelbaum, and R. W. Tsien. 1979. Three-microelectrode voltage clamp experiments in calf cardiac Purkinje fibers: is slow inward current inadequately measured? *J. Physiol. (Lond.)*. 290:201–225.

Kass, R. S., and R. W. Tsien. 1982. Fluctuations in membrane current driven by intracellular calcium in cardiac Purkinje fibers. *Biophys. J.* 38:259–269.

Latorre, R., and C. Miller. 1983. Conduction and selectivity in potassium channels. *J. Membr. Biol.* 71:11–30.

Lee, K. S., and R. W. Tsien. 1982. Reversal of current through calcium channels in dialyzed single heart cells. *Nature (Lond.)*. 297:498–501.

Lee, K. S., and R. W. Tsien. 1983 Mechanism of calcium channel block by verapamil, D600, diltiazem, and nitrendipine in single dialyzed heart cells. *Nature (Lond.)*. 302:790–794.

Levenberg, K. A. 1944. A method for the solution of certain nonlinear problems in least squares. *Appl. Math. Comput.* 2:164–168.

Marquardt, D. W. 1963. An algorithm for least-squares estimation of nonlinear parameters. *J. Soc. Ind. Appl. Math.* 11:431–441.

McDonald, T. F., and W. Trautwein. 1978. The potassium current underlying delayed rectification in cat ventricular muscle. *J. Physiol. (Lond.)*. 274:217–246.

McGuigan, J. A. S. 1974. Some limitations of the double sucrose gap, and its use in a study of the slow current in mammalian ventricular muscle. *J. Physiol. (Lond.)*. 240:775–806.

Meier, C. F., and B. G. Katzung. 1981. Cesium blockade of delayed outward currents and electrically induced pacemaker activity in mammalian ventricular myocardium. *J. Gen. Physiol.* 77:531–547.

Murphy, E., J. F. Aiton, C. R. Horres, and M. Lieberman. 1983. Calcium elevation in cultured heart cells: its role in cell injury. *Am. J. Physiol.* 245:C316-C321.

Noble, D., and R. W. Tsien. 1968. The kinetics and rectifier properties of the slow potassium current in cardiac Purkinje fibres. *J. Physiol. (Lond.)*. 195:185–213.

Noble, D., and R. W. Tsien. 1969. Outward membrane currents activated in the plateau range of potentials in cardiac Purkinje fibres. *J. Physiol. (Lond.)*. 200:205–231.

Noble, D., and R. W. Tsien. 1972. The repolarization of heart cells. *In* Electrical Phenomena in Heart. W. C. deMello, editor. Academic Press, Inc., New York.

Noble, S. F. 1976. Potassium accumulation and depletion in frog atrial muscle. *J. Physiol. (Lond.)*. 258:579–613.

Noma, A., and H. Irisawa. 1976. A time- and voltage-dependent potassium current in the rabbit sinoatrial node cell. *Pfluegers Arch. Eur. J. Physiol.* 366:251–258.

Ojeda, C., and O. Rougier. 1974. Kinetic analysis of the delayed outward currents in frog atrium. Existence of two types of preparations. *J. Physiol. (Lond.)*. 239:51–73.

Ralston, A., M. S. Wilf. 1960. Mathematical Methods for Digital Computers. John Wiley & Sons, Inc., New York.

Reuter, H. 1979. Properties of two inward membrane currents in the heart. *Annu. Rev. Physiol.* 41:413–424.

Reuter, H., and H. Scholz. 1977. A study of the ion selectivity and the kinetic properties of the calcium dependent slow inward current in mammalian cardiac muscle. *J. Physiol. (Lond.)*. 264:17–47.

Reuter, H., and C. F. Stevens. 1980. Ion conductance and ion selectivity of potassium channels in snail neurons. *J. Membr. Biol.* 57:103–118.

Sanguinetti, M. C., and R. S. Kass. 1984. Voltage-dependent block of calcium channel current in the calf cardiac Purkinje fiber by dihydropyridine calcium channel antagonists. *Circ. Res.* 55:336–348.

Scheuer, T., and R. S. Kass. 1983. Phenytoin reduces calcium current in the cardiac Purkinje fiber. *Circ. Res.* 53:16–23.

Sheu, S. S., M. Korth, D. A. Lathrop, and H. Fozzard. 1980. Intra- and extracellular K^+ and Na^+ activities and resting membrane potential in sheep cardiac Purkinje strands. *Circ. Res.* 47:692–700.

Siegelbaum, S. A., and R. W. Tsien. 1980. Calcium-activated outward current in calf cardiac Purkinje fibres. *J. Physiol. (Lond.)*. 299:485–506.

Stevens, C. F. 1978. Interactions between intrinsic membrane protein and electric field: an approach to studying nerve excitability. *Biophys. J.* 22:295–306.

Wier, W. G., A. A. Kort, M. D. Stern, E. G. Lakatta, and E. Marban. 1983. Cellular calcium fluctuations in mammalian heart: direct evidence from noise analysis of aequorin signals in Purkinje fibers. *Proc. Natl. Acad. Sci. USA*. 80:7367–7371.